Enhanced Single-Photon Emission from Carbon-Nanotube Dopant States Coupled to Silicon Microcavities

Akihiro Ishii,[†,‡] Xiaowei He,[§] Nicolai F. Hartmann,[§] Hidenori Machiya,[†,‖] Han Htoon,[§] Stephen K. Doorn,[§] and Yuichiro K. Kato*,[†,‡]

[†]Nanoscale Quantum Photonics Laboratory, RIKEN, Saitama 351-0198, Japan

[‡]Quantum Optoelectronics Research Team, RIKEN Center for Advanced Photonics, Saitama 351-0198, Japan

[§]Center for Integrated Nanotechnologies, Materials Physics and Applications Division, Los Alamos National Laboratory, Los Alamos, New Mexico 87545, United States

[‖]Department of Electrical Engineering, The University of Tokyo, Tokyo 113-8656, Japan

S *Supporting Information*

ABSTRACT: Single-walled carbon nanotubes are a promising material as quantum light sources at room temperature and as nanoscale light sources for integrated photonic circuits on silicon. Here, we show that the integration of dopant states in carbon nanotubes and silicon microcavities can provide bright and high-purity single-photon emitters on a silicon photonics platform at room temperature. We perform photoluminescence spectroscopy and observe the enhancement of emission from the dopant states by a factor of ∼50, and cavity-enhanced radiative decay is confirmed using time-resolved measurements, in which a ∼30% decrease of emission lifetime is observed. The statistics of photons emitted from the cavity-coupled dopant states are investigated by photon-correlation measurements, and high-purity single photon generation is observed. The excitation power dependence of photon emission statistics shows that the degree of photon antibunching can be kept high even when the excitation power increases, while the single-photon emission rate can be increased to ∼1.7 × 10^7 Hz.

KEYWORDS: Carbon nanotubes, photoluminescence, single-photon source, diazonium doping, photonic crystal
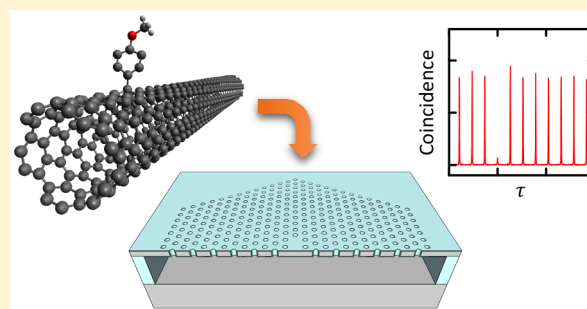
S ingle-photon emitters are a fundamental element for quantum information technologies,[1] and a wide range of materials has been explored to obtain ideal single-photon-emitting devices.[2] In particular, semiconducting single-walled carbon nanotubes (SWCNTs) are regarded as a promising material for such an application because they are a nanoscale light-emitting material[3] having stable excitonic states that arise from the one-dimensional structure of SWCNTs.[4,5] Under cryogenic temperatures, excitons in SWCNTs are localized and behave as quantum-dot-like states,[6] exhibiting a quantum light signature.[7,8] At room temperature, single-photon generation using SWCNTs has already been accomplished by two approaches.[9−13] The first is where exciton trapping sites are created to localize excitons,[10,11] and the second is where efficient exciton−exciton annihilation process is used to reduce the number of mobile excitons to unity.[12,13] The approach using exciton trapping sites allows for high-purity single-photon generation, the use of chirality-sorted SWCNTs, and the direct deposition on various types of substrates. Furthermore, trapping sites protect excitons from quenching sites in SWCNTs, and optically allowed defect states appear below the dark states of E_{11} excitons, resulting in a significant brightening of photoluminescence (PL).[14,15] Recently, aryl sp^3

defects have received considerable attention because of the wide range of selectability of SWCNT chiralities, dopant species, and reaction conditions, which allows for tunable emission wavelength and decay lifetime.[16] Using this method, single-photon generation with a purity of 99% and an emission wavelength of 1550 nm is achieved at room temperature.[11]

For practical single-photon sources, not only single-photon purity and operating temperature but also emission wavelength, line width, brightness, and photon-extraction efficiency are important. From this aspect, cavity structures are widely used to improve the performance of single-photon emitters.[17−19] As for SWCNT single photon emitters, photonic[20,21] and plasmonic[22] cavity configurations have been used to enhance the brightness of single photon emission at low temperatures. Further development is expected by integrating single photon emitters into silicon photonics because it can lead to on-chip integrated quantum devices,[23] and SWCNTs have a potential for such an application due to their emission wavelengths having low transmission losses in silicon. Microcavities on silicon substrates

have been used to enhance photoluminescence[24,25] and Raman[26] signals, and efficient coupling, even to a single carbon nanotube, has also been achieved,[27−29] demonstrating that SWCNTs are suitable for integration with silicon photonics.

Here, we report on integration of SWCNT dopant-state emitters with silicon microcavities. Emission from aryl sp^3 defect states in SWCNTs coupled to two-dimensional photonic crystal microcavities is characterized by PL microscopy, and a significant enhancement of PL intensity is observed. Time-resolved PL measurements on the same device show a direct evidence of enhanced emission decay rates by the Purcell effect, and we confirm single-photon emission from the device by performing photon correlation measurements. Despite the fact that we expect multiple emitters within our excitation spot, we observe clear antibunching. The zero-delay second-order intensity correlation $g^{(2)}(0)$ is as low as 0.1, showing high-purity single-photon generation, and the value is stable even at high-power excitation, which allows for single-photon emission rates as high as ∼1.7×10^7 Hz.

We start sample preparation by fabrication of photonic crystal microcavities on a silicon-on-insulator substrate (Figure 1a). We use the shift-L3 cavities, which consist of three missing holes with two slightly shifted holes in a line.[30] Electron beam lithography defines the photonic crystal pattern, and the 200 nm thick top Si layer is etched through by dry etching. The buried SiO_2 layer with a thickness of 1000 nm is then etched by 20 wt % hydrofluoric acid, and thermal oxidation is performed at 900 °C for an hour to form a 10 nm thick SiO_2 layer on the top Si layer. A scanning electron micrograph of a typical device is shown in Figure 1b. Doped carbon nanotubes are prepared from chirality-enriched (6,5) SWCNTs encapsulated in a sodium deoxycholate (DOC) surfactant. Aryl functionalization is done using a diazonium dopant (4-methoxybenzenediazonium, MeO−Dz); details are provided in the literature.[31] We dilute the doped SWCNT solution with water to avoid the bundling or piling up of SWCNTs on a substrate, and finally, the solution is drop-cast on the devices using a glass micropipette.

PL measurements are performed with a home-built sample-scanning confocal microscopy system.[13] We use a Ti:sapphire laser in which the output can be switched between continuous-wave (CW) and ∼100 fs pulses with a repetition rate of 76 MHz. We use an excitation wavelength of 855 nm, which matches the phonon sideband absorption for (6,5) SWCNTs.[32] The excitation laser beam with a power P is focused onto the sample by an objective lens with a numerical aperture of 0.85. PL, and the reflected beams are collected by the same objective lens and separated by a dichroic filter. A Si photodiode detects the reflected beam for imaging, while a translating mirror is used to switch between PL spectroscopy and time-resolved PL measurements. PL spectra are measured with an InGaAs photodiode array attached to a spectrometer. For time-resolved measurements, E_{11} emission at around 1000 nm is filtered out by a wavelength-tunable band-pass filter with a transmission window of 10 nm or a long-pass filter with a cut-on wavelength of 1100 nm. Fiber-coupled two-channel superconducting single photon detector (SSPD) connected to a 50:50 signal-splitting fiber is used to perform PL decay and photon correlation measurements. All measurements are conducted at room temperature in a nitrogen-purged environment.

We perform automated collection of PL spectra[33] at all cavity positions to find devices with good optical coupling. For a device in which a significant enhancement of the dopant state
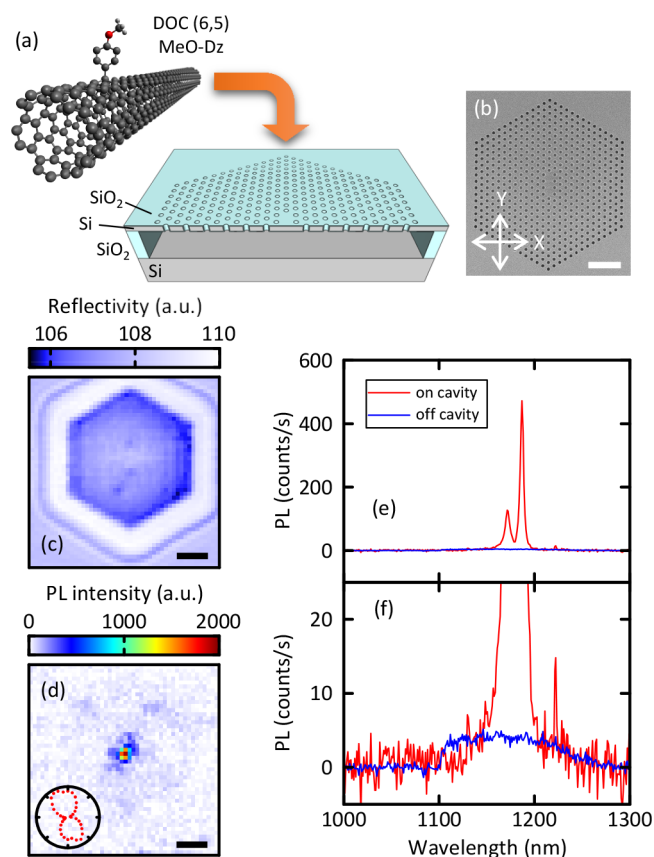

Figure 1. (a) Schematic images of a doped SWCNT and a photonic crystal microcavity. (b) A scanning electron micrograph of a photonic crystal microcavity. The arrows define the directions of X and Y polarization for excitation. (c) Reflectivity and (d) PL images. The inset in panel d is the laser polarization dependence of PL intensity on the cavity. For panel d and its inset, PL intensity is obtained by integrating PL over a 10 nm wide spectral window centered at 1187 nm. (e) PL spectra taken on the cavity (red) and off the cavity (blue). (f) An enlarged view of the low-intensity region of the data shown in panel e. (b−d) The scale bars are 2 μm. (c−f) Y-polarized CW laser with $P = 1$ μW is used for excitation. (e, f) The long-pass filter with a cut-on wavelength of 1100 nm is used when the off-cavity spectrum is taken.

(E_{11}*) emission[16] is observed, reflectivity and PL images are taken (Figure 1c,d). The enhanced PL is localized at the center of the cavity, as expected from PL enhancement due to coupling with the resonance modes of the cavity. In Figure 1e,f, PL spectra on and off the cavity are shown in which the on-cavity signal is taken at the center of the cavity, while the off-cavity spectrum is measured within the photonic crystal pattern but away from the cavity position. PL spectrum on the cavity shows multiple sharp peaks, while broad emission is observed at the off-cavity position. At the on-cavity position, emission from dopant states is enhanced at the cavity mode wavelengths, and therefore, the overall spectral shape reflects the cavity modes. At the off-cavity position, however, a broad spectrum results from an ensemble of dopant states. In the on-cavity spectrum, the peak showing the highest intensity at an emission wavelength of 1187 nm has a full-width at half-maximum of 3.9 nm, corresponding to a quality factor $Q = 300$. We assign the highest-intensity peak to the second mode of the L3 cavity.[34] In the on-cavity and off-cavity PL spectra, we obtain an enhancement factor of ∼50 by comparing the PL intensities

integrated over a 10 nm wide spectral window centered at 1187 nm.

The PL enhancement can become large as there are other cavity-induced effects in addition to the Purcell effect. In our devices, it is known that localized guided modes can increase the excitation by more than a factor of 50,[34] and coupling to such an absorption resonance can explain the strong excitation polarization dependence (inset of Figure 1d). Furthermore, the directionality of the cavity radiation can improve the PL collection efficiency by as much as a factor of 4.[35] Combined with the Purcell effect, these cavity effects can significantly brighten the nanotube emitters, and thus, the obtained enhancement factor of ~50 would be a reasonable result.

To investigate the Purcell enhancement of the radiative decay rate, we perform time-resolved PL measurements on the same device shown in Figure 1c–f. For on-cavity PL, a single peak is spectrally filtered by tuning the transmission wavelength of the band-pass filter to reject other modes and uncoupled emission (Figure 2a), while the long-pass filter is used instead
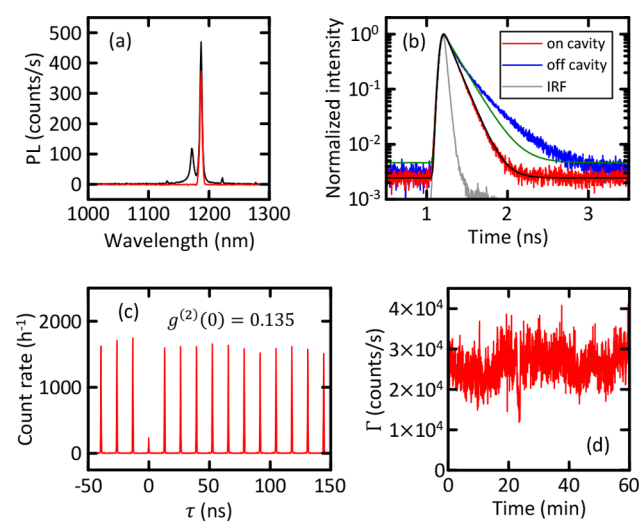
Figure 2. (a) PL spectra on the cavity taken before (black) and after (red) the band-pass filter is set. CW laser with P = 1 μW is used for excitation. (b) PL decay curves taken with pulsed laser excitation at P = 0.1 μW. The red and blue lines are for the on-cavity and typical off-cavity data, respectively. Fits with a convoluted monoexponential decay function are also shown for the on the cavity (black curve) and off the cavity (green curve) data. The gray solid line represents the IRF. (c, d) An intensity-correlation histogram and a time trace of photon-detection rate, respectively, taken on the cavity at P = 0.5 μW. An integration time of 1 s is used for each data point in panel d. (a–d) A Y-polarized laser is used for excitation. All of the measurements are performed at room temperature.

for off-cavity PL to obtain the average lifetime of the dopant-state ensemble. In Figure 2b, PL decay curves taken at the on-cavity and off-cavity positions are shown, and fits are performed using a monoexponential decay function convoluted with a Gaussian profile representing the instrument response function (IRF) of the system. Although PL decay of doped SWCNTs typically exhibits a biexponential curve,[11,16] here, we use a monoexponential decay for simplicity. From the fits, we obtain the on-cavity PL lifetime τ_{on} = 122.0 ± 0.2 ps and the off-cavity PL lifetime τ_{off} = 173.8 ± 0.4 ps. If we assume the radiative quantum efficiency η of 2.4%, which is estimated by the unaffected quantum efficiency of ~11% for MeO–Dz doped (6,5) SWCNTs in water[14] and PL quenching by a factor of

~4.5 caused by an interaction with the SiO$_2$ substrate,[11] the ~30% reduction of the emission lifetime corresponds to a Purcell factor of $F_p = (\tau_{off}/\tau_{on}-1)\,\eta^{-1} = 18$, a coupling factor $\beta = F_p/(1 + F_p) = 0.95$, and an enhanced radiative quantum efficiency of 31%.

We perform such lifetime measurements on 10 other devices and obtain an average lifetime of 131.2 ps with a standard deviation of 43.8 ps. The lifetime varies on different devices, suggesting that coupling is affected by some uncontrolled factors. Coupling efficiency is in general affected by spectral overlap, spatial overlap, and polarization overlap between the emitters and cavity modes. Moreover, SWCNT density fluctuations may have a significant effect in our samples. We note that variations in the cavity quality factors are not the main reason because the Q of dopant-state emission is much lower than that of the cavity peak.

Next, we measure photon correlation for the same cavity peak shown in Figure 2a,b, and clear photon antibunching is observed, as shown in Figure 2c. We evaluate the normalized second-order intensity correlation at zero time delay $g^{(2)}(0)$ from the intensity correlation histogram by subtracting the dark counts and binning each peak with a binning width of 2 ns. We note that the histogram is taken within a time window from −60 to 300 ns, and side peaks after a time delay τ = 60 ns are used for normalization to avoid under-estimation due to photon bunching. For the data shown in Figure 2c, we obtain $g^{(2)}(0)$ = 0.136 ± 0.005, indicating high-purity single-photon emission.

It is surprising that we obtain such high-purity single photon emission from a sample with drop-casted SWCNTs, in which numerous emitters are expected within the laser spot. In fact, by counting the number of individual bright spots in a wide-field PL image in which more-diluted solution is drop-cast, we estimate the density of dopant-state emitters to be roughly 1–10 μm^{-2}. One explanation is that cavity coupling and spectral filtering allow selective photon collection from a few number of emitters. In fact, we actually observe higher $g^{(2)}(0)$ when the band-pass filter is removed (Supporting Information S1). It is worth mentioning that we could not measure photon correlation of off-cavity signal as the emission intensity is too low, indicating the advantages of cavity coupling.

During the photon correlation measurements, time traces of the photon detection rate are also recorded (Figure 2d). The total photon detection rate Γ, defined as the sum of detection rates at the two channels, is obtained from the intensity correlation count rate C using the relation:

$$\Gamma = \left(\sqrt{r} + \frac{1}{\sqrt{r}}\right)\sqrt{\frac{C}{T}} \tag{1}$$

where r is the signal splitting ratio between the two channels, and T = 353.7 ns is the effective time window for the 27 peaks that are included in the correlation histograms (Supporting Information S2). In Figure 2d, the PL intensity shows a relatively large fluctuation over time, with a standard deviation ~23 times larger than that of shot-noise limited fluctuation. We observe such intensity fluctuation of the cavity-coupled peak for all devices we have measured, which may be caused by the influence of the substrate.[20]

Finally, we investigate excitation power dependence of photon emission statistics on three other devices. The PL spectra on the cavities with and without the band-pass filter are shown in Figure 3a–c. For these spectrally filtered peaks, we
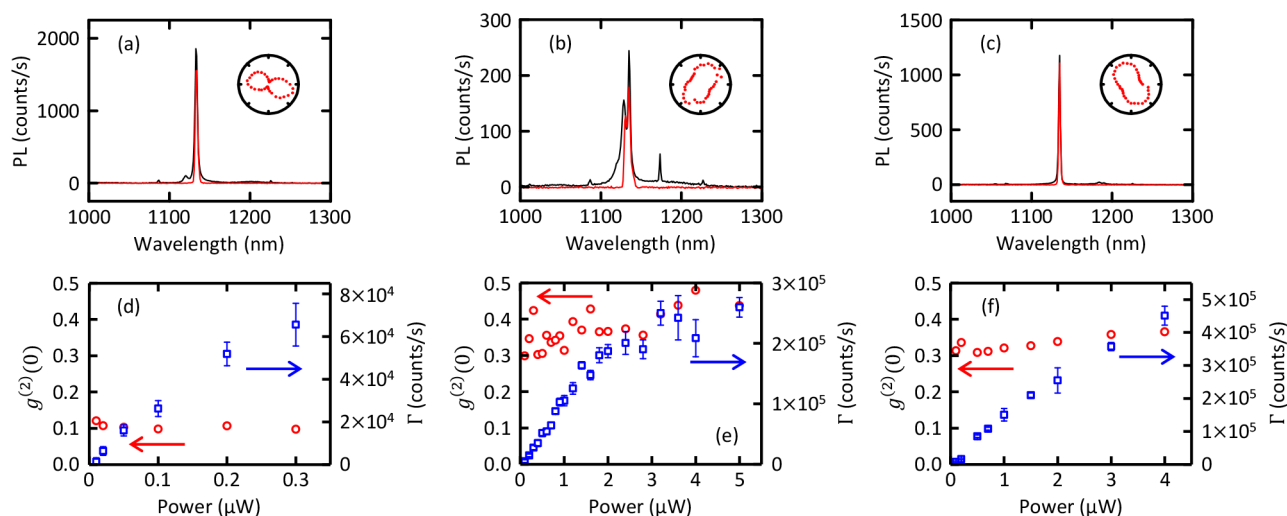
Figure 3. (a−c) PL spectra of three different devices taken on the cavities before (black) and after (red) the band-pass filter is set. The filter is tuned to the highest intensity peaks, where we assign the modes at (a) 1133 nm to the second mode, (b) 1135 nm to the second mode, and (c) 1135 nm to the fifth mode. Insets show the laser polarization dependence of the PL intensity for each peak. A CW laser with $P = 1\ \mu W$ is used for excitation. (d−f) Excitation power dependence of $g^{(2)}(0)$ (red circles) and Γ (blue squares). Data shown in panels d−f are obtained from devices whose PL spectra are shown in panels a−c, respectively. A pulsed laser is used for excitation. Error bars are the standard deviation of Γ obtained by analyzing the time-trace data for each data point. For $g^{(2)}(0)$, error bars are not shown because they are smaller than the symbols in almost all of the data points. For panels a and d, an X-polarized laser is used, while a Y-polarized laser is used for panels b and c and panels e and f.

measure $g^{(2)}(0)$ and Γ (Figure 3d−f) while increasing P until Γ shows a rapid drop, which indicates the deterioration of the devices. As P increases, Γ increases linearly, while $g^{(2)}(0)$ remains almost constant, except for the high-power region in Figure 3e, where Γ saturates and $g^{(2)}(0)$ slightly increases. In all devices, $g^{(2)}(0)$ remains lower than 0.5 throughout the range of P, indicating the robustness of the quantum light signature. This behavior parallels the previous report[11] in which defect states for SWCNTs on a polymer film can also show excellent $g^{(2)}(0)$ values even at relatively high pump powers. At $P = 4\ \mu W$ in Figure 3f, we obtain the highest Γ of 4.5×10^5 counts per second. We note that clear bunching is observed when P is high (Supporting Information S3), which may be caused by an increase of background signals from SWCNTs that are not coupled to the cavity mode.

In the four devices for which we have measured the photon statistics, we find a positive correlation between single-photon purity and the degree of polarization ρ, which is defined by:

$$\rho = \frac{I_{max} - I_{min}}{I_{max} + I_{min}} \qquad (2)$$

where I_{max} and I_{min} are the highest and lowest PL intensity, respectively, obtained by fitting the excitation polarization dependence to a sine function (insets of Figure 1d and Figure 3a−c). For the two devices whose $g^{(2)}(0)$ are shown in Figure 2c and Figure 3d, we obtain $g^{(2)}(0) \approx 0.1$ and $\rho \approx 0.8$, while $g^{(2)}(0) \approx 0.35$ and $\rho \approx 0.6$ are obtained for the other two devices. This correlation is reasonable because low ρ implies that the SWCNT axis and the localized guided mode polarization do not match or that multiple SWCNTs with different orientations are coupling to the same mode of the cavity. This observation suggests that controlling the SWCNT density and orientation on the cavities is a key factor in obtaining high-quality single-photon-emitting devices.

The obtained values of Γ can be converted to actual photon emission rates at the devices using the total photon collection efficiency in our optical system, which is estimated to be ~2.6%

(Supporting Information S4). For the highest photon detection rate, $\Gamma = 4.5 \times 10^5$ counts per second in our measurements, we obtain the corresponding photon emission rate of $\sim 1.7 \times 10^7$ photons per second. Dividing by the laser pulse repetition rate of 7.6×10^7 Hz, the photon emission rate corresponds to the single photon emission efficiency of ~22%, which is consistent with the estimated quantum efficiency by the lifetime shortening observed in time-resolved measurements. Compared to the previously reported value for similar aryl-functionalized SWCNTs but wrapped by PFO-bpy and deposited onto a Au-deposited substrate with a separation layer of 160 nm thick polystyrene,[11] the single-photon emission efficiency is almost two times higher.

For achieving further improvement of our devices, the optimization of SWCNT concentration is a key factor, as mentioned above. Lowering the SWCNT density to an individual SWCNT level will produce an ideal situation for cavity coupling, but such a low density of SWCNTs results in an extremely low yield of cavity-coupled devices. Once appropriate conditions for SWCNT deposition are determined, spin-coating can be used to obtain a more-uniform and more-reproducible deposition of SWCNTs on cavities,[24] which enables the fabrication of integrated quantum-light emitters on silicon chips. As another approach, position-controlled limited-area deposition using a micropipette or nanodroplet[36,37] may yield better results because it does not degrade the cavity quality, although such small-volume SWCNT deposition only at the cavity positions is challenging in practice. The improvement of cavity-coupling efficiency by avoiding quenching from substrates may be possible by using a thinner and more-efficient separation layer, such as hexagonal boron nitride thin films.[38] In addition, the relationship between coupling efficiency and cavity modes is worth investigating, such that the quality factor and mode profile are different depending on the mode order.[39,40] Larger mode volumes are beneficial for obtaining coupling to SWCNTs on the substrate but result in a lower Purcell effect at the same time. Finally, we comment on

the tunability of our devices. The emission wavelength of aryl-functionalized SWCNTs can be tuned by selecting chiralities and dopant species,[11,16] and photonic crystal microcavities have a high flexibility for both absorption and emission resonances.[34] Our approach should therefore lead to bright single-photon emitters at 1550 nm. In principle, it should also be possible to obtain indistinguishable single photon sources at room temperature by using higher-quality cavities.

In summary, we demonstrate integration of carbon-nanotube dopant-state emitters with silicon microcavities, and the PL characteristics and photon statistics of the devices are investigated. PL intensity enhancement by a factor of ∼50 is observed from the dopant-state emission coupled to the cavity mode, and time-resolved measurements reveal a ∼30% lifetime shortening by the Purcell effect on the cavity-coupled emission. Photon correlation measurements are performed on the devices, and we confirm that room-temperature single-photon emission capability, a key feature of sp^3-doped SWCNTs, is preserved in the cavity-enhanced PL emission. We obtain $g^{(2)}(0)$ as low as 0.1 and find that the degree of photon antibunching is stable over a wide range of excitation power. By increasing the excitation power, we obtain a single-photon detection rate as high as 4.5×10^5 Hz, which corresponds to a single-photon emission rate of ∼1.7×10^7 Hz and a single-photon emission efficiency of ∼22% per laser pulse. Our results indicate that integration of dopant-state emitters in SWCNTs with silicon microcavities can provide bright and high-purity quantum-light sources at room temperature on silicon photonics platform, raising expectations toward integrated quantum photonic devices.

ASSOCIATED CONTENT

Ⓢ Supporting Information

The Supporting Information is available free of charge on the ACS Publications website at DOI: 10.1021/acs.nanolett.8b01170.

Additional details on autocorrelation histograms taken with and without the band-pass filter, derivation of Γ, the excitation power dependence of intensity correlation histograms, and the estimation of photon collection efficiency of the system. (PDF)

AUTHOR INFORMATION

Corresponding Author
*E-mail: yuichiro.kato@riken.jp.
ORCID Ⓘ
Xiaowei He: 0000-0002-4982-8250
Nicolai F. Hartmann: 0000-0002-4174-532X
Han Htoon: 0000-0003-3696-2896
Stephen K. Doorn: 0000-0002-9535-2062
Yuichiro K. Kato: 0000-0002-9942-1459

Notes
The authors declare no competing financial interest.

ACKNOWLEDGMENTS

REFERENCES

(1) O'Brien, J. L.; Furusawa, A.; Vučkovic, J. Photonic quantum technologies. *Nat. Photonics* **2009**, *3*, 687−695.

(2) Aharonovich, I.; Englund, D.; Toth, M. Solid-state single-photon emitters. *Nat. Photonics* **2016**, *10*, 631−641.

(3) Avouris, P.; Freitag, M.; Perebeinos, V. Carbon-nanotube photonics and optoelectronics. *Nat. Photonics* **2008**, *2*, 341−350.

(4) Wang, F.; Dukovic, G.; Brus, L. E.; Heinz, T. F. The Optical Resonances in Carbon Nanotubes Arise from Excitons. *Science* **2005**, *308*, 838−841.

(5) Maultzsch, J.; Pomraenke, R.; Reich, S.; Chang, E.; Prezzi, D.; Ruini, A.; Molinari, E.; Strano, M. S.; Thomsen, C.; Lienau, C. Exciton binding energies in carbon nanotubes from two-photon photoluminescence. *Phys. Rev. B: Condens. Matter Mater. Phys.* **2005**, *72*, 241402.

(6) Hofmann, M. S.; Noé, J.; Kneer, A.; Crochet, J. J.; Högele, A. Ubiquity of Exciton Localization in Cryogenic Carbon Nanotubes. *Nano Lett.* **2016**, *16*, 2958−2962.

(7) Högele, A.; Galland, C.; Winger, M.; Imamoğlu, A. Photon Antibunching in the Photoluminescence Spectra of a Single Carbon Nanotube. *Phys. Rev. Lett.* **2008**, *100*, 217401.

(8) Hofmann, M. S.; Glückert, J. T.; Noé, J.; Bourjau, C.; Dehmel, R.; Högele, A. Bright, long-lived and coherent excitons in carbon nanotube quantum dots. *Nat. Nanotechnol.* **2013**, *8*, 502−505.

(9) Endo, T.; Ishi-Hayase, J.; Maki, H. Photon antibunching in single-walled carbon nanotubes at telecommunication wavelengths and room temperature. *Appl. Phys. Lett.* **2015**, *106*, 113106.

(10) Ma, X.; Hartmann, N. F.; Baldwin, J. K. S.; Doorn, S. K.; Htoon, H. Room-temperature single-photon generation from solitary dopants of carbon nanotubes. *Nat. Nanotechnol.* **2015**, *10*, 671−675.

(11) He, X.; Hartmann, N. F.; Ma, X.; Kim, Y.; Ihly, R.; Blackburn, J. L.; Gao, W.; Kono, J.; Yomogida, Y.; Hirano, A.; Tanaka, T.; Kataura, H.; Htoon, H.; Doorn, S. K. Tunable room-temperature single-photon emission at telecom wavelengths from sp^3 defects in carbon nanotubes. *Nat. Photonics* **2017**, *11*, 577−582.

(12) Ma, X.; Roslyak, O.; Duque, J. G.; Pang, X.; Doorn, S. K.; Piryatinski, A.; Dunlap, D. H.; Htoon, H. Influences of Exciton Diffusion and Exciton-Exciton Annihilation on Photon Emission Statistics of Carbon Nanotubes. *Phys. Rev. Lett.* **2015**, *115*, 017401.

(13) Ishii, A.; Uda, T.; Kato, Y. Room-Temperature Single-Photon Emission from Micrometer-Long Air-Suspended Carbon Nanotubes. *Phys. Rev. Appl.* **2017**, *8*, 054039.

(14) Piao, Y.; Meany, B.; Powell, L. R.; Valley, N.; Kwon, H.; Schatz, G. C.; Wang, Y. Brightening of carbon nanotube photoluminescence through the incorporation of sp^3 defects. *Nat. Chem.* **2013**, *5*, 840−845.

(15) Miyauchi, Y.; Iwamura, M.; Mouri, S.; Kawazoe, T.; Ohtsu, M.; Matsuda, K. Brightening of excitons in carbon nanotubes on dimensionality modification. *Nat. Photonics* **2013**, *7*, 715−719.

(16) Hartmann, N. F.; Velizhanin, K. A.; Haroz, E. H.; Kim, M.; Ma, X.; Wang, Y.; Htoon, H.; Doorn, S. K. Photoluminescence Dynamics of Aryl sp^3 Defect States in Single-Walled Carbon Nanotubes. *ACS Nano* **2016**, *10*, 8355−8365.

(17) Strauf, S.; Stoltz, N. G.; Rakher, M. T.; Coldren, L. A.; Petroff, P. M.; Bouwmeester, D. High-frequency single-photon source with polarization control. *Nat. Photonics* **2007**, *1*, 704.

(18) Englund, D.; Shields, B.; Rivoire, K.; Hatami, F.; Vučković, J.; Park, H.; Lukin, M. D. Deterministic Coupling of a Single Nitrogen Vacancy Center to a Photonic Crystal Cavity. *Nano Lett.* **2010**, *10*, 3922−3926.

(19) Kaupp, H.; Hümmer, T.; Mader, M.; Schlederer, B.; Benedikter, J.; Haeusser, P.; Chang, H.-C.; Fedder, H.; Hänsch, T. W.; Hunger, D.

Purcell-Enhanced Single-Photon Emission from Nitrogen-Vacancy Centers Coupled to a Tunable Microcavity. *Phys. Rev. Appl.* **2016**, *6*, 054010.

(20) Walden-Newman, W.; Sarpkaya, I.; Strauf, S. Quantum Light Signatures and Nanosecond Spectral Diffusion from Cavity-Embedded Carbon Nanotubes. *Nano Lett.* **2012**, *12*, 1934−1941.

(21) Jeantet, A.; Chassagneux, Y.; Raynaud, C.; Roussignol, P.; Lauret, J. S.; Besga, B.; Estève, J.; Reichel, J.; Voisin, C. Widely Tunable Single-Photon Source from a Carbon Nanotube in the Purcell Regime. *Phys. Rev. Lett.* **2016**, *116*, 247402.

(22) Luo, Y.; Ahmadi, E. D.; Shayan, K.; Ma, Y.; Mistry, K. S.; Zhang, C.; Hone, J.; Blackburn, J. L.; Strauf, S. Purcell-enhanced quantum yield from carbon nanotube excitons coupled to plasmonic nano-cavities. *Nat. Commun.* **2017**, *8*, 1413.

(23) Harris, N. C.; Bunandar, D.; Pant, M.; Steinbrecher, G. R.; Mower, J.; Prabhu, M.; Baehr-Jones, T.; Hochberg, M.; Englund, D. Large-scale quantum photonic circuits in silicon. *Nanophotonics* **2016**, *5*, 456.

(24) Watahiki, R.; Shimada, T.; Zhao, P.; Chiashi, S.; Iwamoto, S.; Arakawa, Y.; Maruyama, S.; Kato, Y. K. Enhancement of Carbon Nanotube Photoluminescence by Photonic Crystal Nanocavities. *Appl. Phys. Lett.* **2012**, *101*, 141124.

(25) Noury, A.; Roux, X. L.; Vivien, L.; Izard, N. Enhanced light emission from carbon nanotubes integrated in silicon micro-resonator. *Nanotechnology* **2015**, *26*, 345201.

(26) Sumikura, H.; Kuramochi, E.; Taniyama, H.; Notomi, M. Cavity-enhanced Raman scattering of single-walled carbon nanotubes. *Appl. Phys. Lett.* **2013**, *102*, 231110.

(27) Imamura, S.; Watahiki, R.; Miura, R.; Shimada, T.; Kato, Y. K. Optical Control of Individual Carbon Nanotube Light Emitters by Spectral Double Resonance in Silicon Microdisk Resonators. *Appl. Phys. Lett.* **2013**, *102*, 161102.

(28) Miura, R.; Imamura, S.; Ohta, R.; Ishii, A.; Liu, X.; Shimada, T.; Iwamoto, S.; Arakawa, Y.; Kato, Y. K. Ultralow mode-volume photonic crystal nanobeam cavities for high-efficiency coupling to individual carbon nanotube emitters. *Nat. Commun.* **2014**, *5*, 5580.

(29) Machiya, H.; Uda, T.; Ishii, A.; Kato, Y. K. Spectral tuning of optical coupling between air-mode nanobeam cavities and individual carbon nanotubes. *Appl. Phys. Lett.* **2018**, *112*, 021101.

(30) Akahane, Y.; Asano, T.; Song, B.-S.; Noda, S. High-Q photonic nanocavity in a two-dimensional photonic crystal. *Nature* **2003**, *425*, 944.

(31) Hartmann, N. F.; Yalcin, S. E.; Adamska, L.; Haroz, E. H.; Ma, X.; Tretiak, S.; Htoon, H.; Doorn, S. K. Photoluminescence imaging of solitary dopant sites in covalently doped single-wall carbon nanotubes. *Nanoscale* **2015**, *7*, 20521−20530.

(32) Vora, P. M.; Tu, X.; Mele, E. J.; Zheng, M.; Kikkawa, J. M. Chirality dependence of the K-momentum dark excitons in carbon nanotubes. *Phys. Rev. B: Condens. Matter Mater. Phys.* **2010**, *81*, 155123.

(33) Ishii, A.; Yoshida, M.; Kato, Y. K. Exciton diffusion, end quenching, and exciton-exciton annihilation in individual air-suspended carbon nanotubes. *Phys. Rev. B: Condens. Matter Mater. Phys.* **2015**, *91*, 125427.

(34) Liu, X.; Shimada, T.; Miura, R.; Iwamoto, S.; Arakawa, Y.; Kato, Y. K. Localized Guided-Mode and Cavity-Mode Double Resonance in Photonic Crystal Nanocavities. *Phys. Rev. Appl.* **2015**, *3*, 014006.

(35) Fujita, M.; Takahashi, S.; Tanaka, Y.; Asano, T.; Noda, S. Simultaneous Inhibition and Redistribution of Spontaneous Light Emission in Photonic Crystals. *Science* **2005**, *308*, 1296−1298.

(36) Galliker, P.; Schneider, J.; Eghlidi, H.; Kress, S.; Sandoghdar, V.; Poulikakos, D. Direct printing of nanostructures by electrostatic autofocussing of ink nanodroplets. *Nat. Commun.* **2012**, *3*, 890.

(37) Kress, S. J. P.; Richner, P.; Jayanti, S. V.; Galliker, P.; Kim, D. K.; Poulikakos, D.; Norris, D. J. Near-Field Light Design with Colloidal Quantum Dots for Photonics and Plasmonics. *Nano Lett.* **2014**, *14*, 5827−5833.

(38) Kim, K. K.; Hsu, A.; Jia, X.; Kim, S. M.; Shi, Y.; Dresselhaus, M.; Palacios, T.; Kong, J. Synthesis and Characterization of Hexagonal Boron Nitride Film as a Dielectric Layer for Graphene Devices. *ACS Nano* **2012**, *6*, 8583−8590.

(39) Chalcraft, A. R. A.; Lam, S.; O'Brien, D.; Krauss, T. F.; Sahin, M.; Szymanski, D.; Sanvitto, D.; Oulton, R.; Skolnick, M. S.; Fox, A. M.; Whittaker, D. M.; Liu, H.-Y.; Hopkinson, M. Mode structure of the L3 photonic crystal cavity. *Appl. Phys. Lett.* **2007**, *90*, 241117.

(40) Fujita, M.; Tanaka, Y.; Noda, S. Light Emission From Silicon in Photonic Crystal Nanocavity. *IEEE J. Sel. Top. Quantum Electron.* **2008**, *14*, 1090−1097.